Mechanism of the phase transitions in MnAs

J. Łażewski,* P. Piekarz, and K. Parlinski
Institute of Nuclear Physics, Polish Academy of Sciences, Radzikowskiego 152, 31-342 Kraków, Poland
(Received 13 July 2010; revised manuscript received 28 October 2010; published 17 February 2011)

Based on first-principles calculations, the structural, magnetic, dynamic properties, and the α-hexagonal $\rightarrow$ β-orthorhombic $\rightarrow$ γ-hexagonal phase transitions of ferromagnetic, antiferromagnetic, and paramagnetic MnAs are studied. The phonon-dispersion curves for some of the phases were derived using the direct method. Soft modes were found in ferromagnetic and antiferromagnetic structures in a wide range of pressures. A strong dependence of the soft-mode energy on the magnetic moment and magnetic order was revealed. The double-well potential was found as a function of the soft-mode amplitude at the reduced crystal volume. In the β-orthorhombic phase, a new antiferromagnetic configuration consisting of linear chains of alternating spins was found. Therefore, the mechanism of the magnetostructural phase transitions confirms the antiferromagnetic or paramagnetic (with antiferromagnetic fluctuations) state of the β-orthorhombic phase. The paramagnetic γ-hexagonal phase is stabilized at high temperature in the displacive second-order phase transition owing to the disappearance of the soft mode.

DOI: 10.1103/PhysRevB.83.054108 PACS number(s): 75.30.Sg, 31.15.es, 63.20.dk

I. INTRODUCTION

The magnetic properties of MnAs have been known for a long time.[1] In recent years, MnAs has attracted the attention of researchers owing to its possible magnetocaloric[2] and spintronic applications.[3] A giant magnetocaloric effect (MCE) observed in MnAs (Ref. 2) allows for adiabatic heating up and cooling down materials by applying the external magnetic field. It provides a mechanism of magnetic refrigeration at room temperature. The MCE is connected with the magnetostructural properties of MnAs, resulting from the unique interplay of magnetic and lattice degrees of freedom.[4,5]

At ambient conditions, MnAs crystallizes in a hexagonal NiAs-type structure (α phase), which transforms into a orthorhombic MnP-type structure (β phase) at approximately $T_c = 315$ K.[6] This structural transition is associated with the change in magnetic state from the ferromagnetic (FM) in the α phase to the paramagnetic (PM) in the β phase. Because of the magnetostructural coupling, the $\alpha \rightarrow \beta$ transition is of first order with a discontinuous change of volume ($\sim$2%),[7] resistivity, and magnetization. A large latent heat[8] and hysteresis of the phase transition[9,10] has been observed. At higher temperature $T_t = 393$ K, in the second-order phase transition, the crystal structure reverts back to the hexagonal symmetry (γ phase), which is PM.[11]

The exceptional magnetic properties of MnAs, including the giant MCE,[2] magnetoresistance,[12] and magnetoelastic effects[13] are induced by the first-order magnetostructural transition. At ambient pressure, the entropy change reaches 30 J/(kg K), and this value increases further upon compression.[14] As found by Zou *et al.*,[15] the majority of the total entropy change comes from the magnetic transition, and the contribution from the lattice is very small. Above T_c, the magnetization drops to zero, however, the magnetic susceptibility does not show a typical PM behavior (it increases with temperature). The Curie-Weiss dependence is observed only above T_t.

All of these experimental facts indicate an existing connection between the magnetic and structural properties of MnAs. The first phenomenological model of the $\alpha \rightarrow \beta$ transition was proposed by Bean and Rodbell,[8] who considered the explicit dependence of the critical temperature T_c on volume. Goodenough *et al.* proposed the mechanism based on the high-spin to the low-spin state transition induced by crystal distortion.[9] Both phase transitions were studied within the Landau theory with two coupled order parameters: lattice distortion and magnetization.[16–19] This model successfully described a complex phase diagram with the first-order and second-order coexistence lines, including the effect of the magnetic field. On a microscopic level, the magnetostructural properties of MnAs were studied within the density functional theory (DFT).[20–25] In particular, it was demonstrated that the orthorhombic distortion in the β phase induces the antiferromagnetic (AFM) order at the reduced crystal volume.[24,25] The second-order phase transition ($\beta \rightarrow \gamma$) was explained as the effect of stabilization of the hexagonal phase at a larger volume owing to thermal expansion.[25] These studies clearly indicated the importance of the lattice distortion in both phase transitions, and the significant spin-lattice coupling in MnAs.

A phonon spectrum in MnAs has not been measured yet, however, there are many indications that phonons are involved in both phase transitions in MnAs. The anomalous behavior of elastic constants close to the structural phase transition was interpreted in terms of a condensation of a soft mode.[26,27] Similarly, the temperature dependence of the Debye-Waller factor at T_c suggests the critical lowering of phonon frequencies.[28] A soft-mode mechanism of the magnetostructural transition was also postulated on the basis of general thermodynamic considerations.[15] In the previous study, we have explicitly demonstrated the existence of the soft mode in the hexagonal phase, which could have induced the phase transition to the orthorhombic symmetry.[29] The soft mode strongly interacts with magnetic moments, and it explains in a natural way the magnetoelastic properties of MnAs.

In this paper, we extend the lattice dynamics studies and present in detail the phonon spectra for both the hexagonal and orthorhombic phases. We focus on the properties of the

soft mode, relating its behavior with the mechanism of the phase transitions in MnAs. The paper is organized as follows. In Sec. II, we describe the calculation methods. The crystal structure as a function of pressure is discussed in Sec. III. In Sec. IV A, we present the phonon spectra for both crystal structures of MnAs. Section IV B contains information on the soft mode, and Sec. IV C describes the coupling between the soft mode and magnetic structure. In Sec. V, we discuss the mechanism of phase transitions in MnAs. Finally, the main conclusions are presented in Sec. VI.

II. CALCULATION SETUP

We have performed first-principles calculations based on the spin-polarized DFT as implemented in the Vienna *ab initio* simulation package (VASP).[30] The calculations have been performed using the full-potential projector-augmented wave method[31] within the generalized gradient approximation (GGA) approach.[32,33] The following valence base configurations have been included: Mn $3d^5 4s^2$ and As $4s^2 4p^3$. The integration in the **k**-point space has been sampled by the $4 \times 4 \times 4$ Monkhorst-Pack mesh,[34] and the energy cutoff for the plane-wave expansion was equal to 320 eV. The crystal structure has been optimized using the conjugate gradient technique with the energy convergence criteria set at 10^{-8} and 10^{-5} for the electronic and ionic iterations, respectively. For the hexagonal and orthorhombic symmetry we used $2 \times 2 \times 1$ and $1 \times 2 \times 1$ supercells, respectively, both with 16 atoms and periodic boundary conditions. Larger supercells with 72 and 96 atoms in the hexagonal and orthorhombic structures have been used for checking the convergence of the lattice parameters and phonon frequencies.

Phonon dispersions have been calculated with the direct method[35] as implemented in the PHONON program.[36] The force constants and dynamical matrix have been obtained from the Hellmann-Feynman forces calculated with small individual displacements of nonequivalent atoms. For FM order, there exist six independent displacements for both hexagonal and orthorhombic phases. For the PM phase all atoms should be considered as nonequivalent, which led to 48 independent displacements. For better accuracy, each displacement has been made with a positive and negative sign. To study the dependence of phonon frequencies on magnetic moments, the difference between the "up" and "down" state occupations has been fixed during VASP calculations.

III. THE GROUND STATE AT $T = 0$

MnAs in a broad range of temperature and pressure coexists in two phases: α-MnAs hexagonal ($P6_3/mmc$, 194) and β-MnAs with orthorhombic ($Pnma$, 62) unit cells.[10] Increasing twice the unit-cell volume of the α phase by doubling the area on the hexagonal plane ($a^{\text{ortho}} = \sqrt{3}a^{\text{hex}}$, $b^{\text{ortho}} = c^{\text{hex}}$, and $c^{\text{ortho}} = a^{\text{hex}}$), one can obtain the β-phase unit cell. Because the orthorhombic space group is a subgroup of the hexagonal one, there may exist—from the structural point of view—a continuous transformation between these phases. It is reflected in the experimental observation that for a temperature interval from 0 to 150 K the hysteresis region extends from normal pressure up to 3.6 kb. For higher temperatures and low pressures (below 2 kb) the hexagonal phase becomes more stable. Above 313 K, the orthorhombic phase is more stable, however, at 393 K the reentrance of the hexagonal phase is observed. The existence of a large hysteresis region as well as the return of the hexagonal phase in high temperature indicate a small difference in the free energies of both phases. Also small differences in lattice parameters and volumes reported in literature confirm this hypothesis.

We have optimized the crystal structure of MnAs in both symmetries, assuming the FM order on Mn atoms. For the hexagonal structure, we obtained the lattice parameters $a = 3.666$ Å and $c = 5.508$ Å, in a good agreement with the experimental data taken at $T = 110$ K, $a_{\text{exp}} = 3.733$ Å, and $c_{\text{exp}} = 5.677$ Å. With increasing temperature, a drops slightly to 3.724 Å at room temperature, while c increases its value to 5.707 Å. Comparing to the experimental magnetic moment on Mn atoms ($3.4\mu_B$), we obtained a smaller value, $3.05\mu_B$, for the optimized hexagonal structure, however, for the experimental values of lattice constants we found $3.35\mu_B$.

The relaxation in the orthorhombic symmetry with FM ordering of spins leads to a very similar structure (the difference in atomic positions is less than 0.01 Å), which can be described using the pseudohexagonal lattice parameters. The pseudohexagonal structure is defined by an additional (third) lattice constant b (related to the hexagonal parameter a) and by a pseudohexagonal angle α with values close to 120°. The differences in total energies of both structures are less for the FM one by 0.01 eV per one supercell (16 atoms). It confirms that the ground state with the FM order has the hexagonal symmetry.

In order to study the relative stability of both phases, we have repeated calculations in a wide range of pressures, from −50 to 40 kb. The negative pressures correspond to larger volumes, which can imitate the crystal thermal expansion or the effect of substitution of atoms with larger radius.[37] In Fig. 1, we present the lattice parameters for both hexagonal

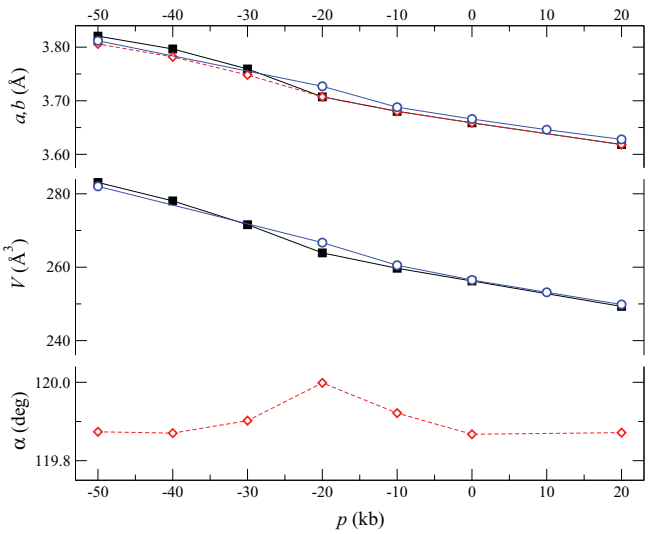

FIG. 1. (Color online) Calculated lattice parameters and volume as functions of pressure for the hexagonal (open circles) and orthorhombic (filled squares) structures. Parameters recalculated for the pseudohexagonal structure were depicted by open diamonds.

and orthorhombic structures as functions of pressure. For the orthorhombic phase, the pseudohexagonal structure was introduced to emboss the changes of lattice constants and angles (open diamonds in Fig. 1). At $p = 0$ and all positive pressures, the lattice constant and volumes of both phases are identical. However, there is a small deviation (not exceeding 0.15°) from the hexagonal angle (120°) in the orthorhombic structure. Interestingly, this angle approaches 120° at $p = -20$ kb, and then decreases again with more negative pressure. There is also a small difference between the values of lattice parameter a; the highest observed at −20 kb reads 0.54%. At the same pressure the difference in the volumes is equal to 1%. The relative difference in the volumes induced by an external pressure between −50 and 20 kb is very similar for both structures and is equal 11%.

One can conclude that keeping the FM order unchanged, the crystal optimization in two different supercells relevant for the hexagonal and orthorhombic symmetries leads in practice to the hexagonal structure. It confirms that the FM configuration in the hexagonal phase is a ground state at $T = 0$. It also proves that only volume changes within the FM configuration cannot explain the magnetostructural phase transition in MnAs. The same conclusions result from the previous *ab initio* studies.[24,25]

In the framework of collinear calculations, apart from the FM configuration, one can study antiferromagnetically ordered systems as well. We consider two different AFM arrangements: one, called AFM(1), with the magnetic moments aligned antiparallel in the a-b plane and with the same directions of moments between the a-b planes, and the other, AFM(2), with parallel magnetic moments in the a-b plane and with staggered magnetic orientations between the nearest a-b planes. In agreement with the previous study,[24,25] the AFM systems have a higher energy than the FM one, smaller volumes, and reduced magnetic moments. In Table I, we put together their characteristics for pressures for 0 and 20 kb. Additionally, the AFM order in MnAs induces the orthorhombic distortion observed in the β phase.[24,25] This effect will be discussed in the following sections.

The dependence of magnetic moments on crystal volume for the FM and AFM states is plotted in Fig. 2. In the range of pressure considered, magnetic moments change linearly with volume. The magnitudes of moments in the AFM state are systematically lower (∼10%) than in the FM one. The AFM(3) case will be discussed in detail later.

TABLE I. Volumes, enthalpies, and magnetic moments for antiferromagnetically ordered systems in comparison with data for the FM configuration.

	$p = 0$			$p = 20$ kb		
	V (Å^3)	H (eV)	m (μ_B)	V (Å^3)	H (eV)	m (μ_B)
FM	256.52	−113.300	3.05	249.85	−110.142	2.93
AFM(1)	253.20	−112.903	2.86	247.22	−109.783	2.74
AFM(2)	246.98	−113.037	2.72	241.30	−109.993	2.61

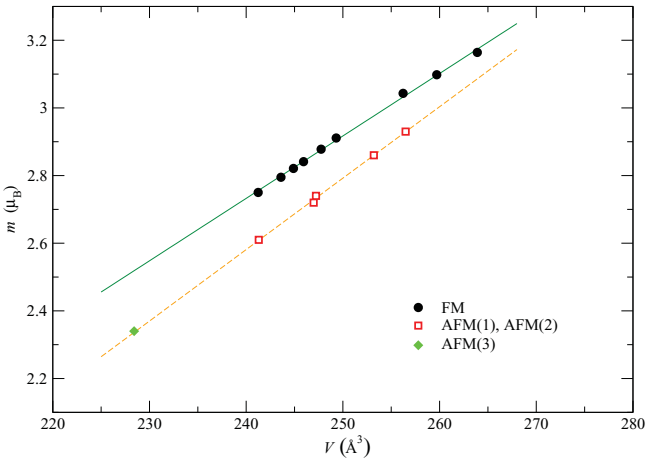

FIG. 2. (Color online) Dependence of magnetic moment on crystal volume.

IV. PHONONS

A. Dispersion curves

In this section, we present the phonon spectra obtained for the hexagonal and orthorhombic structures. Because the primitive unit cell for the hexagonal symmetry contains four atoms, the complete phonon spectrum consists of 12 dispersion curves: three acoustical and nine optical ones. A group-theoretical analysis shows that the nine zone-center optical modes are classified by the following symmetries: $A_{2u} + B_{1g} + B_{2u} + E_{1u} + E_{2g} + E_{2u}$. The E modes are doubly degenerate. Only the E_{2g} mode is Raman active, while the A_{2u} and E_{1u} modes are infrared active.

For the orthorhombic phase with eight atoms in a primitive unit cell, there exist 24 dispersion curves, and the optical modes are split among the following symmetries: $4A_g + 2A_u + 2B_{1g} + 3B_{1u} + 4B_{2g} + B_{2u} + 2B_{3g} + 3B_{3u}$. All *gerade* modes are Raman active. Additionally, B_u modes are infrared active. Phonon frequencies obtained at the Γ point in both structures are presented in Table II. It is worth pointing out that the volume of the first Brillouin zone (BZ) for the orthorhombic structure is two times smaller than for hexagonal structure, and the high-symmetry point M of the latter one becomes the Γ point of orthorhombic BZ. For that reason we put the phonon frequencies for the hexagonal system also at the M point and assign them to the proper values obtained for the orthorhombic system.

The calculated phonon-dispersion relations for the FM hexagonal phase along the high-symmetry directions for different pressures are plotted in Fig. 3. At $p = 0$, all phonon energies are positive, which ensures the dynamical stability of the hexagonal phase in ambient conditions. For positive pressure, most dispersion curves shift to higher energies owing to increased interatomic forces. With the crystal expansion, phonon energies decreases. The opposite effect is seen for the lowest mode at the M point, which strongly goes down upon compression. This soft mode will be discussed in detail in the next section.

The phonon spectrum for the FM orthorhombic phase is presented in Fig. 4. In the broad range of pressures, all phonon frequencies are positive, which shows that the

TABLE II. Assignment of the calculated frequencies at the Γ point in the hexagonal and orthorhombic structures. Values from the second column, $\omega(M)$, correspond to the frequencies at the M point of the hexagonal Brillouin zone, which in the orthorhombic structure becomes the Γ point. For phonons at the Γ point, the mode symmetry and their activity (R—Raman, I—infrared) for optically active modes has been given. Doubly degenerated hexagonal phase modes of E symmetry split into two one-dimensional modes in the orthorhombic phase. All presented values are in THz.

$P6_3/mmc$			$Pnma$	
$\omega(\Gamma)$	$\omega(M)$	Symm. (activ.)	$\omega(\Gamma)$	Symm. (activ.)
	1.133		0.943	A_g (R)
	2.847		2.912	B_{1g} (R)
	4.449		4.419	B_{2g} (R)
	4.576		4.593	B_{1u} (I)
4.944		B_{1g}	4.972	B_{2g} (R)
	5.131		5.184	A_u
	5.190		5.216	B_{3g} (R)
5.307		E_{2g} (R)	5.269	A_g (R)
			5.398	B_{3g} (R)
	5.414		5.397	A_g (R)
5.545		E_{2u}	5.491	A_u
			5.623	B_{3u} (I)
	5.505		5.533	B_{3u} (I)
	5.533		5.588	B_{2g} (R)
6.189		A_{2u} (I)	6.256	B_{3u} (I)
6.627		B_{2u}	6.690	B_{1u} (I)
	6.987		7.002	A_g (R)
	7.018		7.049	B_{1g} (R)
7.247		E_{1u} (I)	7.288	B_{2u} (I)
			7.363	B_{1u} (I)
	7.680		7.738	B_{2g} (R)

orthorhombic symmetry cannot be further reduced by the soft-mode mechanism. There is one mode at the Γ point with the A_g symmetry, which strongly depends on pressure. Unlike all other phonons, this mode increases its energy with the crystal expansion. This mode corresponds to the soft mode at the M point in the hexagonal structure.

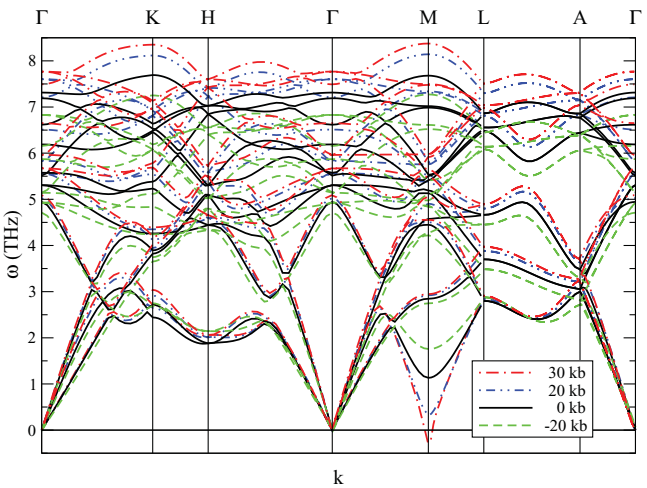

FIG. 3. (Color online) Phonon dispersions for the FM hexagonal phase calculated under pressure.

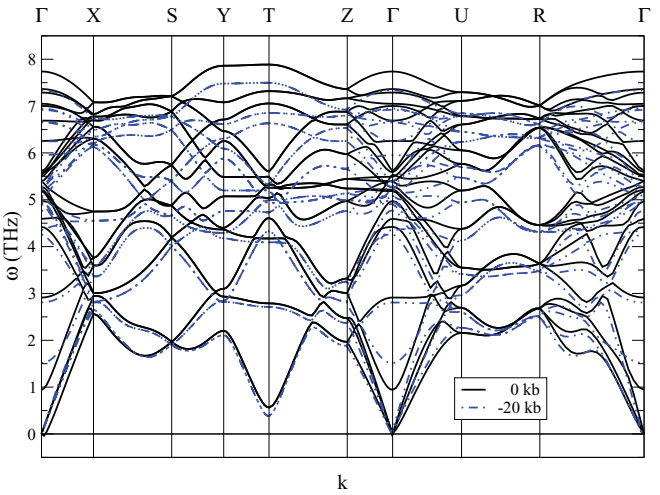

FIG. 4. (Color online) Calculated phonon spectrum in the FM orthorhombic phase.

B. Soft mode

In the Landau theory of structural phase transitions, the normal mode of the soft phonon plays a role of the order parameter. In a typical second-order transition, the soft mode reduces the high-symmetry space group to one of its subgroups, and the order parameter is characterized by the irreducible representation of the high-symmetry space group. Therefore, we can define the order parameter as a vector $\Gamma_{\mathbf{k},j}(\eta_i)$, where $\mathbf{k}$ is a wave vector of the irreducible star, j is the index of ray representations, and η_i are the components of the order parameter. Defined in this way, the order parameter determines uniquely the lattice distortion observed in the phase transition. In the following, we shall denote the soft-mode order parameter by η.

In MnAs, the hexagonal space group $P6_3/mmc$ is reduced to the orthorhombic subgroup $Pnma$ by the irreducible representation M_2^+ at the wave vector $\mathbf{k} = (0.5,0,0)$ (in units of the reciprocal space).[29,38] The atomic displacements associated with the soft mode are presented in Fig. 5. Mn atoms are displaced primarily in the hexagonal a-b planes, so the nearest Mn-Mn distance becomes shorter. As atoms are

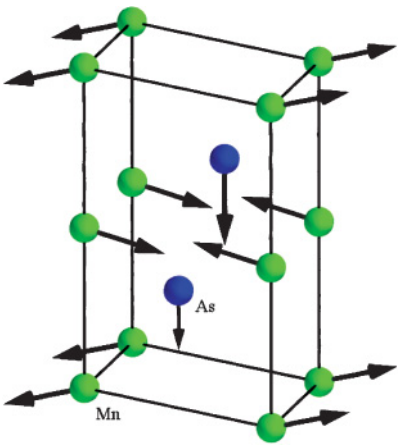

FIG. 5. (Color online) Displacements of atoms in the soft mode at the M point of the hexagonal phase Brillouin zone.

TABLE III. Volume and soft-mode frequency calculated for the hexagonal phase versus external pressure.

p (kb)	V (Å^3)	V/V_0	ω_{soft} (THz)
−50	282.04	1.099	2.280
−20	266.71	1.040	1.756
−10	260.53	1.016	1.333
0	256.52	1.000	1.133
10	253.15	0.987	0.760
20	249.85	0.974	0.322
30	246.73	0.962	−0.277
40	243.95	0.951	−0.546

shifted along the c direction. These atomic displacements are consistent with the orthorhombic distortion observed in the single-crystal x-ray diffraction[6] and with those considered in previous studies.[25]

We have investigated the behavior of the soft mode in a wide range of pressures. The frequencies of the soft mode and the crystal volumes for all considered pressures are presented in Table III. The frequency of the soft mode becomes imaginary for a pressure p_c just above 20 kb. This point could have defined the structural transition from the hexagonal to the orthorhombic phase in the continuous (second-order) phase transition. However, in this particular case—owing to the strong spin-phonon coupling (described below)—magnetic disordering responsible for volume shrinkage considerably decreases transition pressure. The 2% volume collapse accompanying magnetic disordering in the first-order phase transition results in sufficient phonon softening to enforce symmetry reduction and structural transformation.

Next, we study how the total energy changes with the crystal distortion induced by the soft mode. The positions of the atoms have been generated using the polarization vectors of the soft mode obtained at different pressures. In Fig. 6 we have plotted the total energy as a function of the Mn fractional displacement u_{Mn}. At the equilibrium volume ($p = 0$), the energy changes monotonically with the amplitude, showing the quadratic (harmonic) dependence. With increasing pressure this dependence becomes more flat, and at the critical

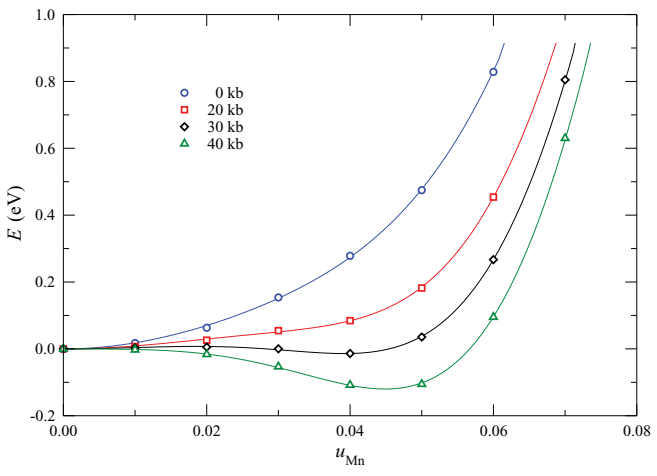

FIG. 6. (Color online) Total energy of MnAs calculated for increasing amplitude of the soft mode as a function of pressure.

TABLE IV. Calculated thermal displacement for hexagonal phase in ambient pressure.

atom	$\sqrt{\langle u^2 \rangle}$ (Å)	Temp. (K)
Mn	0.047	0
	0.095	300
As	0.039	0
	0.077	300

pressure p_c a new minimum appears at approximately $u_{\text{Mn}} = 0.045$. This minimum defines a new position of the Mn atoms in the distorted orthorhombic phase. Such behavior is typical for the displacive phase transition with a condensing soft mode. The atomic shifts from the positions in the ideal hexagonal structure measured at $T = 328$ K are in the range 0.02–0.26 Å.[6] They are comparable to the average thermal displacements calculated from the phonon density of states (Table IV). Interestingly, the local atomic shifts studied by the extended x-ray absorption fine structure (EXAFS) are below the theoretical thermal displacements.[28] It could explain the broad hysteresis region observed in MnAs at low temperatures.

C. The effect of magnetic disordering on phonons

1. Spin-phonon coupling

In the previous section, we have demonstrated that the reduced volume (under pressure) induces the soft mode, which lowers the hexagonal symmetry to the orthorhombic one. Taking into account a considerable dependence of the magnetic moment in the FM phase on volume (see Fig. 2), one can expect a strong coupling between magnetic moments and the soft mode. This coupling has been studied in two different ways. First, we have calculated the phonon-dispersion curves for systems (fully relaxed each time) with reduced values of the magnetic moment m on Mn atoms (at $p = 0$). The obtained dispersions for a few values of m are shown in Fig. 7. For the reduced moment, the same mode at the M point softens and goes to zero at approximately $m \sim 2.6\mu_B$. Such a strong influence of magnetic moments on the soft mode results mainly

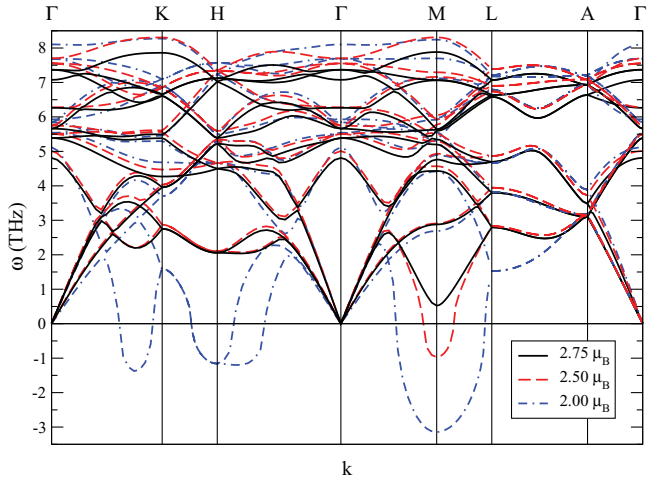

FIG. 7. (Color online) Calculated phonon spectrum in the hexagonal phase for different values of magnetic moment on Mn atoms.

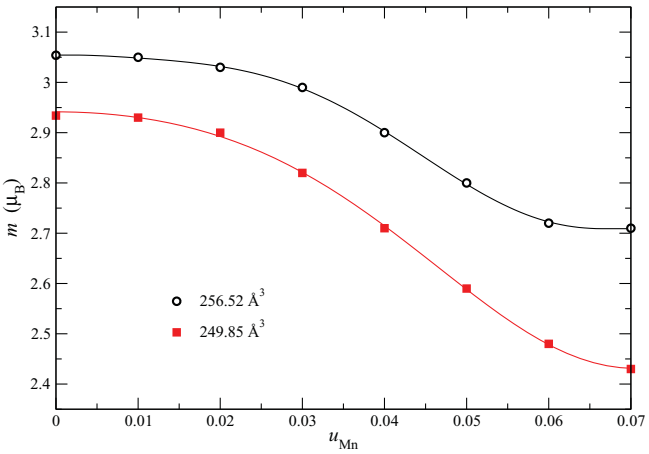

FIG. 8. (Color online) Influence of soft-mode distortion on Mn magnetic moments.

from a reduction of the Mn-Mn distance owing to volume contraction (see Table III).

Next, we have studied how the soft mode modifies the magnitude of magnetic moments. In Fig. 8, we plot the dependence of the magnetic moment on the fractional displacement of the Mn atoms present in the soft mode u_{Mn}. For small amplitudes (<0.055), the magnetic moment decreases monotonically, showing a quadratic dependence on u_{Mn}, and saturates for larger displacements. This dependence becomes stronger for higher pressures. We have also checked how the magnetic moment depends on individual displacements of Mn and As atoms (see Table V). Interestingly, the shift of only Mn atoms influences the magnetic moment even more strongly than the full soft-mode deformation, and the influence of the As atom movements is rather negligible. It could be easy to understand, taking into account the small contribution of As electrons on the Fermi level.

The dependence of the magnetic moment on the lattice deformation u has been derived within the Landau theory by Pytlik and Zieba,[17]

$$m = m_0(1 - \gamma u^2), \tag{1}$$

where m_0 is a magnetic moment in the hexagonal α phase and γ is a coupling parameter. This quadratic dependence perfectly agrees with the relation presented in Fig. 8. For not too large values of u_{Mn} (<0.055), we have fitted the parabolic function and found γ equals 34.12 and 48.65 for $p = 0$ and $p = 20$ kb, respectively. In this way, the results presented here provide the microscopic validation of the effective Landau theory of phase transitions in MnAs.

TABLE V. Magnetic moments for different displacements present in the normal mode at the M point calculated for Mn and As atom fractional displacements equal to 0.034 and 0.032, respectively, as defined by the soft-mode polarization vector.

p (kb)	None	Mn and As	Mn only	As only
0	3.05	2.99	2.94	3.03
20	2.93	2.82	2.80	2.90

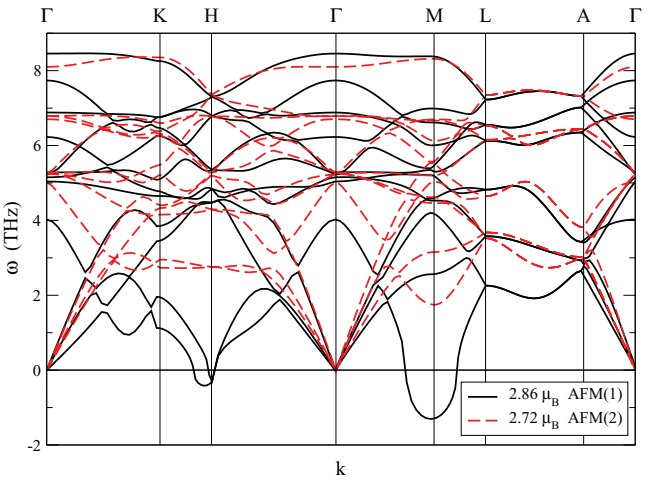

FIG. 9. (Color online) Phonon-dispersion curves calculated in the hexagonal structure for two AFM configurations at zero pressure.

2. *AFM order*

The phonon-dispersion curves obtained at $p = 0$ for two AFM configurations, AFM(1) and AFM(2), are presented in Fig. 9. Because for the AFM order the crystal volume decreases, the whole spectra reach higher frequencies. The most significant difference in comparing to the FM phase at $p = 0$ is the observation of low frequencies, especially at the M point, where the AFM(1) phonon strongly softens while the AFM(2) behaves similarly to the FM phase. This quite surprising feature can be understood by taking into account the specific distribution of atomic displacements in the soft mode (see Fig. 5). Indeed, Mn atoms move in the a-b plane in which the AFM(2) configuration remains FM. In the AFM(1) configuration, the in-plane spins are aligned antiparallel and strongly modify the interatomic forces. It agrees very well with the result, presented in Ref. 25, that only spin configurations with the AFM alignment in the hexagonal planes stabilize the orthorhombic structure. A comparison of the AFM(1) spectrum with the FM one shows that not only the magnetic moment magnitude but also the change of their ordering visibly influences phonon frequencies and can destabilize the hexagonal structure.

In the next step, we study the effect of magnetic disorder on the crystal structure. In principle fully disordered systems cannot be studied in the periodic boundary conditions. Nevertheless, in the 16-atom supercell with eight magnetic Mn atoms, one can randomly orient their magnetic moments in space. We have selected a noncollinear distribution of magnetic moments when the total magnetization equals zero. The starting configuration of local moments is listed in Table VI. Additionally, we have moved all atoms in the supercell according to the pattern of displacements present in the hexagonal-to-orthorhombic phase transition and described by the soft-mode polarization vector. Finally, we have imposed an external pressure of 40 kb under which the FM system is unstable at the M point (see Table III).

After full relaxation of lattice constants and atomic positions (without any symmetry constrains), the crystal symmetry has been examined using the package ISOTROPY.[39] The obtained structure has a *Pnma* orthorhombic symmetry with

TABLE VI. The values of magnetic moments (in μ_B) in the orthorhombic β phase of MnAs before (input) and after (output) structure optimization.

Atom position	Input			Output		
	μ_x	μ_y	μ_z	μ_x	μ_y	μ_z
(0,0,0)	0	0	1	1.15	−0.27	1.97
$(\frac{1}{2},0,0)$	0	1	0	−1.15	0.27	−1.97
$(0,\frac{1}{2},0)$	1	0	0	1.15	−0.27	1.97
$(\frac{1}{2},\frac{1}{2},0)$	0	0	−1	−1.15	0.27	−1.97
$(0,0,\frac{1}{2})$	0	−1	0	1.21	−0.24	1.94
$(\frac{1}{2},0,\frac{1}{2})$	−1	0	0	−1.21	0.24	−1.94
$(0,\frac{1}{2},\frac{1}{2})$	0	1	1	1.21	−0.24	1.94
$(\frac{1}{2},\frac{1}{2},\frac{1}{2})$	0	−1	−1	−1.21	0.24	−1.94

a total magnetic moment smaller than $0.01\mu_B$. The optimized volume, amounting to 228.22 Å^3, is significantly smaller than the corresponding one obtained for the FM configuration under the same pressure (243.95 Å^3). The volume changes ∼6.9%. The equilibrium atomic positions are shifted from the high-symmetry points of the hexagonal structure by vectors presented in Table VII. It should be pointed out that despite a lack of symmetry constraints during the crystal optimization, the resulting structure has an orthorhombic symmetry with high accuracy. It indicates a well-defined minimum of enthalpy (−107.85 eV per 16 atoms unit cell), which is lower than that for the FM phase (−107.06 eV) by ∼50 meV per atom.

In spite of the random initial magnetic configuration, the resulting state shows the AFM order with an arbitrary direction of magnetic alignment (see Table VI). This magnetic state differs from two configurations AFM(1) and AFM(2) discussed before, therefore, we label it AFM(3). The optimized

TABLE VII. The fractional displacements of the Mn and As atoms from the hexagonal high-symmetry positions in the β AFM phase.

u_x	u_y	u_z
	Mn atoms	
0.049	0.025	0.003
−0.049	−0.025	−0.003
0.049	0.025	0.003
−0.049	−0.025	−0.003
−0.049	−0.025	0.003
0.049	0.025	−0.003
−0.049	−0.025	0.003
0.049	0.025	−0.003
	As atoms	
0.002	0.001	−0.054
0.002	0.001	0.054
0.002	0.001	−0.054
0.002	0.001	0.054
−0.002	−0.001	0.054
−0.002	−0.001	−0.054
−0.002	−0.001	0.054
−0.002	−0.001	−0.054

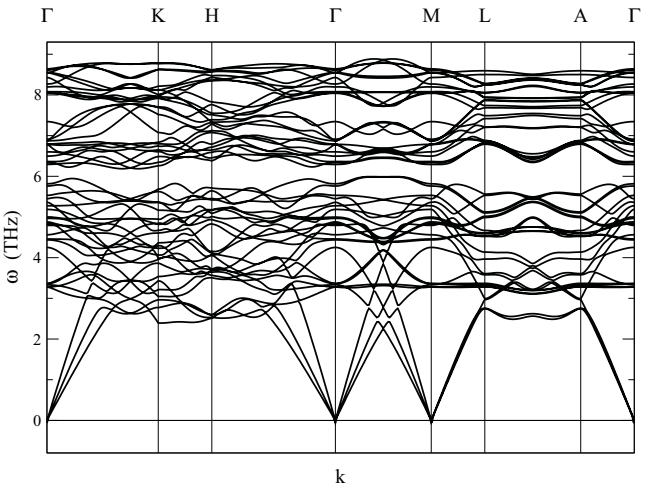

FIG. 10. Phonon-dispersion curves calculated for the AFM(3) orthorhombic structure at $p = 40$ GPa.

magnetic moments on the Mn atoms have a parallel orientation along the line of the $[\frac{\sqrt{3}}{2},\frac{1}{2},0]$ direction and an antiparallel one along the line of the [1,0,0] direction. Along the c direction, the magnetic moments are aligned parallel. Such magnetic ordering consists of alternating chains with parallel spins, which breaks the hexagonal symmetry. In order to verify this result, we have repeated calculations for three different random configurations of magnetic moments. In all cases, we have obtained the AFM(3) state with the same magnetic moment pattern. One should add that this new AFM(3) structure may still diverge from a real magnetic configuration because of the supercell constraints imposed on our calculations.

To check the dynamical stability of the obtained AFM(3) structure, we have calculated its phonon-dispersion curves. Because the calculations were performed without any symmetry constraints, we have had to consider all atoms in the supercell as nonequivalent. As a consequence, we have obtained 48 dispersion curves (see Fig. 10) instead of 24. As it was mentioned above, the M point in the hexagonal structure descends to the Γ point in the orthorhombic phase. Additionally, the points L and A become equivalent.

In Fig. 11, a comparison of the phonon density of states calculated for the orthorhombic AFM(3) and hexagonal FM phases has been presented. Two characteristic features are clearly visible. First, soft phonons at ∼2.2 THz for the FM configuration stiffen in the AFM phase and their average frequency increases up to 3.8 THz. Second, top optical band significantly spreads in the AFM phase, reaching higher frequencies.

V. PHASE TRANSITIONS IN MnAs

In this section, we discuss both phase transitions and the three phases α, β, and γ of MnAs in light of the results obtained in the present work. We found that at $p = 0$ and $T = 0$ the FM hexagonal phase is the most stable. As we have also established, and as has been found in previous DFT studies, the AFM configuration at $p = 0$ and $T = 0$ has a higher energy and induces orthorhombic distortion.[24,25] In addition, we have demonstrated that the AFM hexagonal phase exhibits a soft mode η at the M point. This mode reduces the hexagonal

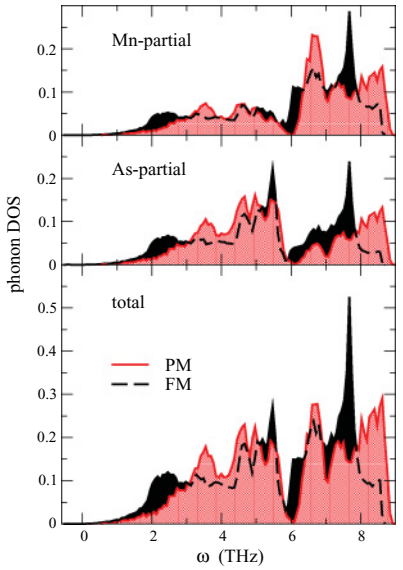

FIG. 11. (Color online) Partial and total phonon density of states for the AFM(3) orthorhombic structure (foreground) and the hexagonal FM structure (background) at $p = 40$ GPa.

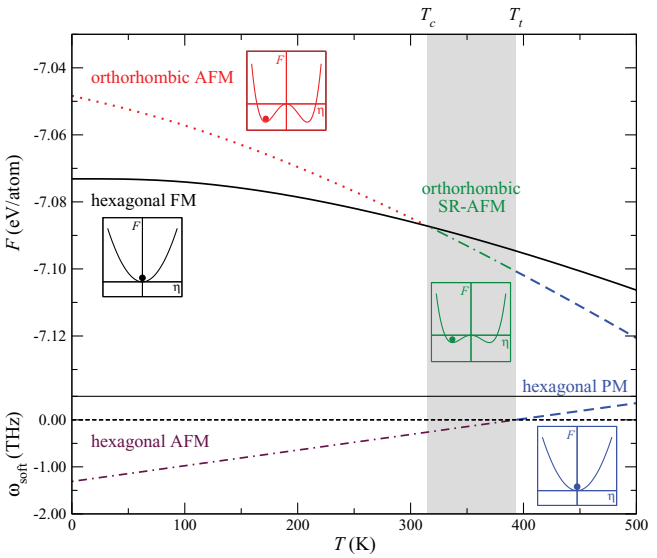

FIG. 12. (Color online) Dependence of the free energy (top) and the soft mode (bottom) on temperature. The calculated F for the FM hexagonal phase was compared with the curve expected for the AFM orthorhombic system. At T_t, thermal expansion stabilized the soft phonon and continuously transforms the orthorhombic phase into the hexagonal phase. Insets: The crystal potential in the respective phases. The region of the stable orthorhombic phase is shown as gray.

crystal symmetry to the orthorhombic structure (see Fig. 9). Furthermore, we have found that the soft mode at the hexagonal FM phase leads also to the orthorhombic phase under external pressure, in agreement with the phase diagram of MnAs.[9]

For $T > 0$, the total free energy $F = E - ST$ consists of internal energy E and entropy S. The main contribution to entropy is expected from the magnetic subsystem, in particular, the entropy of the AFM state is larger than that of the FM state. Hence, the temperature decrease of the free energy is stronger for the AFM system than that of the FM system.

A schematic plot of the free-energy behavior versus temperature is presented in Fig. 12. At the bottom of Fig. 12, we plot the expected temperature dependence of the soft-mode frequency in the AFM state. Here ω_{soft} increases with temperature owing to positive thermal expansion. The free energies of the hexagonal FM and the orthorhombic AFM phases intersect at the point corresponding to the $\alpha \rightarrow \beta$ transition. This transition has a first-order character with a discontinuous jump of the crystal volume. At the moment, an accurate value of T_c cannot be established. The volume decreases across the phase transition as a consequence of a larger specific volume of the FM phase than that of the AFM phase. It should be mentioned that the precise magnetic structure of the β phase is unknown, therefore it could exhibit a more complex magnetic configuration or PM disorder with local AFM fluctuations.[25]

The orthorhombic AFM phase possesses a shallow double-minimum potential that creates conditions for the appearance of critical fluctuations. As a consequence, the short-range order may still be preserved, but the long-range order responsible for the diffraction peaks can gradually disappear when approaching the $\beta \rightarrow \gamma$ phase transition. The magnetic fluctuations are strongly coupled to soft phonons, and a crystal volume change was reported as an abnormal lattice constant increase,[11] Mn-As distance elongation,[37] and observed thermal expansion enhancement.[25] In effect, the short-range order contributes to the entropy and shifts the transition point toward a lower temperature. In the schematic plot of the phase diagram of MnAs presented in Fig. 13, the short-range AFM order in the β phase is denoted as SR-AFM.

The $\beta \rightarrow \gamma$ phase transition is caused by the thermal expansion, which stabilizes the hexagonal structure above T_t. Because the energy of the soft mode, which induces the orthorhombic distortion in the β phase, increases for larger crystal volume (see Fig. 3), it becomes positive ($\eta \rightarrow 0$) at $T = T_t$, as plotted in Fig. 12. Therefore, this is a displacive second-order phase transition occurring owing to the soft mode η, which defines the symmetry change at T_t.[40] In the γ phase, the PM is observed, because the AFM fluctuations found in the orthorhombic phase weaken gradually with increasing temperature and disappear above T_t in the hexagonal structure.

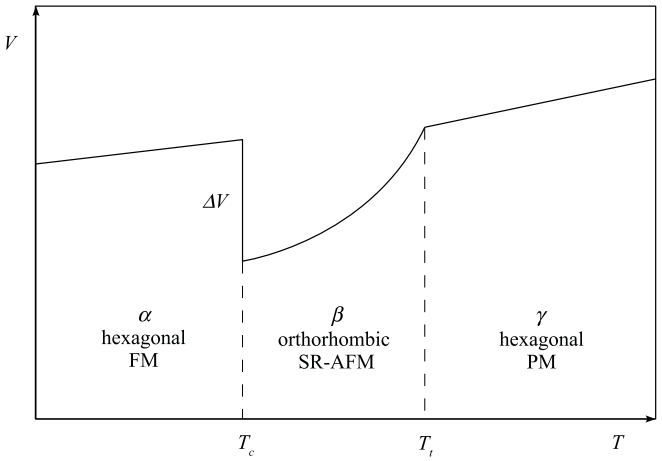

FIG. 13. Phase diagram of MnAs (schematic plot).

The magnetic disordering in the $\alpha \rightarrow \beta$ phase transition is the main reason for the discontinuous change of the crystal volume. Moreover, the volume decrease is related to the reduced magnetic moments owing to the spin-lattice coupling involving the soft mode η (see Fig. 8). Therefore, the spin-phonon coupling plays an important role in the magnetostructural transition. As we discussed above, the entropy change in the magnetostructural transition is mainly caused by the magnetic subsystem. In the previous work,[29] we have estimated the phonon contribution to the entropy change, assuming that the main change of the phonon spectrum is associated with a volume reduction in the $\alpha \rightarrow \beta$ phase transition. A comparison of the phonon entropy between two ferromagnetically ordered systems gave a change $\Delta S_{\mathrm{ph}} = 9.31$ J/(kg K). In the present work, we have gone further and have estimated the phonon entropy change by juxtaposing values for the FM hexagonal and the AFM(3) orthorhombic structures. The obtained entropy jump is ~30% higher than before and reads as 12.42 J/(kg K). However, both estimations are smaller and have an opposite sign to the total entropy change found experimentally. It agrees with the observation that the magnetic contribution to the entropy change is larger than the total one.[15]

VI. SUMMARY

Using the DFT method, we have studied the structural and dynamic properties of the hexagonal and orthorhombic phase of MnAs. We have found continuous changes of lattice parameters and phonon frequencies in a wide range of pressures. In the α phase, there is a soft mode at the M point, which reduces the hexagonal symmetry to the orthorhombic one. We have revealed a strong influence of the magnetic order on the soft-mode frequency and the dynamical stability of the hexagonal phase. This strong spin-phonon coupling plays a crucial role in the mechanism of the magnetostructural transition in MnAs.

ACKNOWLEDGMENTS

The authors would like to express their gratitude to J. Toboła, P. T. Jochym, and M. Sternik for fruitful discussions and critical reading of the manuscript. This work was partially supported by European Community under COST Action P19, and by the Polish government (MNiSW) within Contract No. 44/N-COST/2007/0.

*jan.lazewski@ifj.edu.pl

[1] F. Heuser, Z. Angew. Chem. **17**, 260 (1904); S. Hilpertand and T. Dieckmann, Ber. Dtsch. Chem. Ges. A **44**, 2378 (1911).
[2] H. Wada and Y. Tanabe, Appl. Phys. Lett. **79**, 3302 (2001).
[3] M. Ramsteiner, H. Y. Hao, A. Kawaharazuka, H. J. Zhu, M. Kastner, R. Hey, L. Daweritz, H. T. Grahn, and K. H. Ploog, Phys. Rev. B **66**, 081304(R) (2002).
[4] V. A. Chernenko, L. Wee, P. G. McCormick, and R. Street, J. Appl. Phys. **85**, 7833 (1999).
[5] F. Ishikawa, K. Koyama, K. Watanabe, T. Asano, and H. Wada, J. Phys. Soc. Jpn. **75**, 084604 (2006).
[6] R. H. Wilson and J. S. Kasper, Acta Crystallogr. **17**, 95 (1964).
[7] B. T. M. Willis and H. P. Rooksby, Proc. Phys. Soc. London Sect. B **67**, 290 (1954).
[8] C. P. Bean and D. S. Rodbell, Phys. Rev. **126**, 104 (1962).
[9] J. B. Goodenough and J. A. Kafalas, Phys. Rev. **157**, 389 (1967).
[10] N. Menyuk, J. A. Kafalas, K. Dwight, and J. B. Goodenough, Phys. Rev. **177**, 942 (1969).
[11] T. Suzuki and H. Ido, J. Phys. Soc. Jpn. **51**, 3149 (1982).
[12] J. Mira, F. Rivadulla, J. Rivas, A. Fondado, T. Guidi, R. Caciuffo, F. Carsughi, P. G. Radaelli, and J. B. Goodenough, Phys. Rev. Lett. **90**, 097203 (2003).
[13] F. Iikawa, M. J. S. P. Brasil, C. Adriano, O. D. D. Couto, C. Giles, P. V. Santos, L. Daweritz, I. Rungger, and S. Sanvito, Phys. Rev. Lett. **95**, 077203 (2005).
[14] S. Gama, A. A. Coelho, A. de Campos, A. M. Carvalho, F. C. G. Gandra, P. J. von Ranke, and N. A. de Oliveira, Phys. Rev. Lett. **93**, 237202 (2004).
[15] J. D. Zou, H. Wada, B. G. Shen, J. R. Sun, and W. Li, Europhys. Lett. **81**, 47002 (2008).
[16] I. M. Vitebskii, V. I. Kamenev, and D. A. Yablonskii, Fiz. Tverd. Tela **23**, 215 (1981) [Sov. Phys. Solid State **23**, 121 (1981)].
[17] L. Pytlik and A. Zieba, J. Magn. Magn. Mater. **51**, 199 (1985).
[18] S. K. Asadov, E. A. Zavadskii, V. I. Kamenev, E. P. Stefanovskii, A. L. Sukstanskii, and B. M. Todris, Phys. Solid State **42**, 1696 (2000).
[19] V. I. Val'kov and A. V. Golovchan, Low Temp. Phys. **30**, 711 (2004).
[20] P. Ravindran, A. Delin, P. James, B. Johansson, J. M. Wills, R. Ahuja, and O. Eriksson, Phys. Rev. B **59**, 15680 (1999).
[21] S. Sanvito and N. A. Hill, Phys. Rev. B **62**, 15553 (2000).
[22] A. Continenza, S. Picozzi, W. T. Geng, and A. J. Freeman, Phys. Rev. B **64**, 085204 (2001).
[23] A. Debernardi, M. Peressi, and A. Baldereshi, Mater. Sci. Eng. C **23**, 1059 (2003).
[24] M. K. Niranjan, B. R. Sahu, and L. Kleinman, Phys. Rev. B **70**, 180406(R) (2004).
[25] I. Rungger and S. Sanvito, Phys. Rev. B **74**, 024429 (2006).
[26] K. Barner and H. Berg, Phys. Status Solidi A **49**, 545 (1978).
[27] J. Ihlemann and K. Barner, J. Magn. Magn. Mater. **46**, 40 (1984).
[28] O. Palumbo, C. Castellano, A. Paolone, and R. Cantelli, J. Phys. Condens. Matter **17**, 1537 (2005).
[29] J. Łażewski, P. Piekarz, J. Toboła, B. Wiendlocha, P. T. Jochym, M. Sternik, and K. Parlinski, Phys. Rev. Lett. **104**, 147205 (2010).
[30] G. Kresse and J. Furthmüller, Comput. Mater. Sci. **6**, 15 (1996); Phys. Rev. B **54**, 11169 (1996).
[31] P. E. Blöchl, Phys. Rev. B **50**, 17953 (1994); G. Kresse and D. Joubert, *ibid.* **59**, 1758 (1999).
[32] J. P. Perdew, J. A. Chevary, S. H. Vosko, K. A. Jackson, M. R. Pederson, D. J. Singh, and C. Fiolhais, Phys. Rev. B **46**, 6671 (1992).
[33] J. P. Perdew, K. Burke, and M. Ernzerhof, Phys. Rev. Lett. **77**, 3865 (1996).
[34] H. J. Monkhorst and J. D. Pack, Phys. Rev. B **13**, 5188 (1976).

[35]K. Parlinski, Z. Q. Li, and Y. Kawazoe, Phys. Rev. Lett. **78**, 4063 (1997).
[36]K. Parlinski, PHONON Software, Cracow, 2008, [http://wolf.ifj.edu.pl/phonon/].
[37]A. Zieba, R. Zach, H. Fjellvag, and A. Kjekshus, J. Phys. Chem. Solids **48**, 79 (1987).
[38]H. T. Stokes and D. M. Hatch, *Isotropy Subgroups of the 230 Crystallographic Space Groups* (World Scientific, Singapore, 1988).
[39]H. T. Stokes, D. M. Hatch, and B. J. Campbell, ISOTROPY software, 2007, [http://stokes.byu.edu/isotropy.html].
[40]H. F. Franzen, C. Haas, and F. Jellinek, Phys. Rev. B **10**, 1248 (1974).